Two-step Heating Effect of Hydrochar-MnO_2 Formation and Their Electrochemical Performances

Sekar Tri Wulan Amelia
Department of Chemical Engineering, Faculty of Industrial Technology and System Engineering, Sepuluh Nopember Institute of Technology

Nurtono, Tantular
Department of Chemical Engineering, Faculty of Industrial Technology and System Engineering, Sepuluh Nopember Institute of Technology

Setyawan, Heru
Department of Chemical Engineering, Faculty of Industrial Technology and System Engineering, Sepuluh Nopember Institute of Technology

W. Widiyastuti
Department of Chemical Engineering, Faculty of Industrial Technology and System Engineering, Sepuluh Nopember Institute of Technology

https://doi.org/10.5109/7172256

出版情報：Evergreen. 11 (1), pp.195-206, 2024-03. 九州大学グリーンテクノロジー研究教育センター
バージョン：

Two-step Heating Effect of Hydrochar-MnO_2 Formation and Their Electrochemical Performances

Sekar Tri Wulan Amelia[1], Tantular Nurtono[1], Heru Setyawan[1], W. Widiyastuti[1]*
[1]Department of Chemical Engineering, Faculty of Industrial Technology and System Engineering, Sepuluh Nopember Institute of Technology, Kampus ITS Sukolilo, Surabaya 60111, Indonesia

*Author to whom correspondence should be addressed:
E-mail: widi@chem-eng.its.ac.id

(Received October 17, 2023: Revised February 12, 2024: Accepted March 4, 2024).

Abstract: To improve lignin function in $KMnO_4$ reduction through one-step hydrothermal carbonization (HTC), the HTC method must be modified to produce MnO_2-hydrochar. This study proposed an HTC process with two-step heating to enhance the electrochemical performance of hydrochar. HTC is conducted in two-step heating at 100 °C (4 h) followed by 200 °C (8 h). The highest specific capacitance and kinetic current density of 86.76 F/g and 0.32 mA/cm^2 were obtained from the $KMnO_4$-NH_4OH solution. These findings show that implementing two-step heating in HTC can modify the mechanism and improve the performance of hydrochar.

Keywords: electrocapacitive, electrocatalytic, hydrochar, hydrothermal

1. Introduction

Avocado seeds are well-known for their high antioxidant content. Avocado seeds contain up to 57% of the total antioxidant content found in avocados [1)]. As a result, so many food, drug, and pharmaceutical industries use avocado seeds as a source of antioxidants through extraction. However, in the extraction process, in addition to producing oil, it also generates solid residues in amounts larger than the main product. That is a lignocellulosic waste that must be developed and explored to produce new renewable functional materials to mitigate negative environmental issues [2)]. Utilizing lignocellulosic waste as a carbon-based material is one of the popular strategies in recent years.

Pyrolysis has been developed hundreds of years previously to obtain carbon-based material for various advanced applications. However, to reduce the cost and energy expenses [3)], hydrothermal carbonization (HTC) as an aqueous-based thermochemical method is recently proposed as a promising technology for converting a variety of wet biomasses to carbon material without a pre-drying process, results a high yield, low ash content, and requires a relatively low temperature (180 – 250 °C) [4–6)]. Carbon from the hydrothermal process is called hydrochar. Water at sub- and supercritical conditions contains more ionic compounds than ambient water, which can catalyze the conversion reaction of lignocellulose [7)]. On the other hand, several studies have been conducted using acid/base catalyst or any additional chemicals such as citric acid [5)], acetic acid and potassium hydroxide [6)], ammonia and sulfuric acid [8)], and others. These chemicals have been proven to accelerate the hydrothermal process for converting biomass into hydrochar materials.

However, the chemistry of biomass hydrothermal conversion is well known to be very complex. Hydrolysis, dehydration, and fragmentation of lignin, cellulose, and hemicellulose into derivative monomers such as phenol, 5-HMF, and furfural occur in hydrothermal processes [9)]. This process then continues with the formation of polymerized hydrochar and polyaromatic char. However, some studies have found that the random structure of lignin and its high molecular weight polymers make the lignin reaction mechanism more complex [10)]. Indeed, lignin is thought to interfere with cellulose and hemicellulose hydrolysis at the beginning of the mechanism. Thus, the low lignin content of avocado seed waste provides additional benefits in hydrochar synthesis.

In addition to being dissolved and repolymerized to form hydrochar, lignin can also reduce the $KMnO_4$ precursor through hydrothermal processes [11)]. $KMnO_4$ is widely chosen as the precursor source of the nonprecious metal oxide compound MnO_2, which is in high demand because its high theoretical specific capacitance, high active sites on surface area, low cost, high capacities property, nontoxicity, and ease of synthesis [11–14)]. However, the hydrothermal carbonization process is always completed in one-step within hours at a specific temperature, which cannot control the reduction of $KMnO_4$ by lignin, along with biomass conversion to hydrochar. Lignin is a $KMnO_4$ oxidizer that can be hydrolyzed starting at 200 °C [9,10)]. The reduction of $KMnO_4$ by lignin can occur starting at 80 °C [11)]. Thus, in

the one-step HTC process with a temperature of approximately 200 °C, the lignin structure changes into soluble fragments and converts into hydrocarbons before optimally $KMnO_4$.

From these issues, it is expected that designing of HTC process into a two-step temperature for a particular time can modify the conversion process of lignocellulose along with the reduction of $KMnO_4$ by lignin. As a result, both may occur optimally to produce hydrochar-MnO_2 composites through a series of hydrothermal processes. In this study, temperatures of 100 and 200 °C were selected as two temperature sections for $KMnO_4$ reduction by lignin and lignin conversion into hydrochar, respectively. Moreover, a comparison of one- and two-step heating was conducted to determine its effect on the reaction mechanism of hydrochar-MnO_2 composite formation. In addition, the electrocapacity and electrocatalytic performance of both hydrochars were also studied using different catalysts and heating-steps.

2. Experimental

2.1 Materials

Extracted avocado seed that was collected from solid waste of extraction process, which was done in our previous study (EASP) [15]. The chemicals used are reagent grade of potassium permanganate ($KMnO_4$, 97.5%; UNI-Chem Indonesia), sulfuric acid (H_2SO_4, 96%; Merck), ammonia (NH_4OH, 25%; Merck), and demineralized water (UD. Sumber Ilmiah Persada, Indonesia).

2.2 HTC Experimental

Five grams of EASP were weighed into Teflon-lined designed autoclave stainless-steel hydrothermal reactor with a size of 100 mL. Then, the EASP was mixed with 1 mmol $KMnO_4$ with ratio of 1:10 (w:v) in demineralized water. Furthermore, the effect of acidic and alkaline media on the HTC process was investigated by adding H_2SO_4 (HC-KS) and NH_4OH (HC-KN) into the feedstock solution to achieve the expected pH, which is using universal indicator paper around 2-3 for acidic and 9-10 for alkaline catalyst. Then, the well-sealed reactor was placed in the muffle furnace at the desired operation condition. Next, the reactor was cooled naturally, and the solid was filtered. After obtaining hydrochar, it was rinsed repeatedly until the neutral pH obtained, then dried at temperature of 80 °C for 12 h and weighed. The effect of the heating step on the HTC was studied by varying the HTC process at the one- and two-step heating processes. One-step heating was carried out at 200 °C for 12 h, denoted as (1) that has been done in our previous study [8]. Meanwhile, two-step heating was carried out at 100 °C for 4 h and continued at 200 °C for 8 h, denoted as (2).

2.3 Characterizations

The Brunauer-Emmett-Teller (BET) method (NOVA 1200e, Quantachrome) was used to examine the specific surface area (SSA) and pore characteristics by analyzing the nitrogen adsorption-desorption isotherm. Before the measurements, the samples were degassed for 3 hours in a flow of nitrogen gas at 300 °C. The SSA value was calculated using the multiple-point Brunauer-Emmett-Teller (BET) analysis method. The Barrett Joyner Halenda (BJH) analytical method was used to determine pore diameter and volume.

A scanning electron microscope (SEM, HITACHI FLEXSEM-100) was used to analyze the morphology and pore structure of the hydrochar. The crystalline structures of the hydrochar were studied using a Philips Expert Pro X-ray diffractometer.

2.4 Assay Methods of Electrochemical Performances

A potentiostat-galvanostat (Autolab PGSTAT 302 N, Metrohm) instrument was used to perform cyclic voltammetry (CV) tests in 1 M $Na_2S_2O_3$ aqueous solution to evaluate the electrochemical performances of hydrochar. The samples for the working electrode were then prepared by dispersing them in a weight ratio of 10:1 with poly(vinylidene difluoride) (PVDF) and 1-methyl-2-pyrrolidinone (NMP) as the solvent. The paste was then coated to the surface of nickel foam and cured at temperature of 50 °C. Following proper sample preparation, the CV was measured between 1.0 - 0 V at a scan rate of 10 mV/s (vs. Ag/AgCl).

Then, the samples were mixed with PVdF and NMP for ORR testing as a working electrode. Then, it was dropped over on a glassy carbon electrode (diameter of 3 mm) and dried at approximately of 50 °C. In an O_2-saturated 0.1 M KOH electrolyte, the CV was measured between 1.0 and 1.0 V (vs. Ag/AgCl) at a scan rate of 10 mV/s. The measurement was performed in an O_2 and N_2 saturated 0.1 M KOH electrolyte solution for comparison. The LSV was then done in conjunction with the RDE system to investigate the effect of hydrochar performance on ORR activity. The test was performed at a scan rate of 10 mV/s with a rotating speed range of 400 to 2800 rpm.

3. Results and Discussions

3.1 Raw Material Characteristics

The Chesson-Datta method [16] was used to analyze the lignocellulosic component of the raw material, and the results are shown in our earlier study [8]. This analysis shows the same results as the previous study, that the lignin component of avocado seeds is lower than total cellulose and hemicellulose [17,18]. As a result, these conditions might be contributing to the efficiency of the HTC process because lignin could bother the cellulose and hemicellulose hydrolysis. [10]. More detailed information about lignocellulosic components and proximate analysis of avocado seed is presented in Table 1.

Table 1. Lignocellulosic component and proximate analysis of avocado seed

Component	Composition (%)	Ref.
Lignocellulosic component		8)
Hemicellulose	11.17	
Cellulose	55.13	
Lignin	19.21	
Proximate analysis		19)
Moisture content	13.09	
Dry matter	86.91	
Crude fibre	2.87	
Ash	3.82	

3.2 Visual Appearance of Hydrochar

The visual appearance of hydrochar produced by the HTC process with one- and two-step heating in acid and alkaline catalysts were not much different (Fig. 1). The blackish color of the hydrochar obtained between one- and two-step heating indicates that the carbonization process occurs in HTC with one- and two-step heating processes.

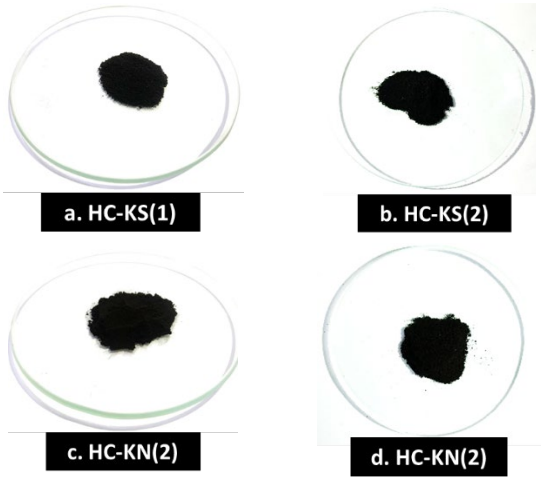

Fig. 1: Visual appearance of hydrochar, HC-KS(1) (a); HC-KS(2) (b); HC-KN(1) (c); and HC-KN(2) (d).

3.3 Yield Analysis

The yields (Table 2) obtained from HTC with one- and two-step heating processes were not significantly different. In all yield analysis results, one-step heating hydrochar yields less than two-step heating. This is due to the decomposition and degradation of lignocellulose components occurring more vigorously at 200 °C with a longer reaction time, which has a substantial impact on hydrochar yield.

Table 2. Hydrochar yield with various feedstock solutions and HTC heating-steps

Code*	Solution	pH**	Temp. (time)	Yield (%)
A	$KMnO_4$-H_2SO_4	2-3	200 °C (12 h)	54.2
B	$KMnO_4$-H_2SO_4	2-3	100 °C (4 h) + 200 °C (8 h)	62.04
C	$KMnO_4$-NH_4OH	9-10	200 °C (12 h)	57.8
D	$KMnO_4$-NH_4OH	9-10	100 °C (4 h) + 200 °C (8 h)	63.6

** sample code of A: HC - KS(1), B: HC - KS(2), C: HC - KN(1), D: HC - KN(2)*

*** pH estimated by using universal pH indicator paper*

3.4 The Morphology and Pore Structure of Hydrochar

SEM images (Fig. 2) show the morphology and pore structure of hydrochar produced with different heating steps. The morphology and pore structure changes between one- and two-step heating HTC using $KMnO_4$-H_2SO_4 (Fig. 2 a-b) look significantly different. A two-step heating HTC process produced sphere-like morphology particles, as shown by the yellow arrow, indicating a more intensive hydrolysis process in two-step heating HTC as the initial mechanism of hydrochar formation [20]. This is also confirmed by the FTIR spectra of hydrochar, which further discuss in the following paragraph.

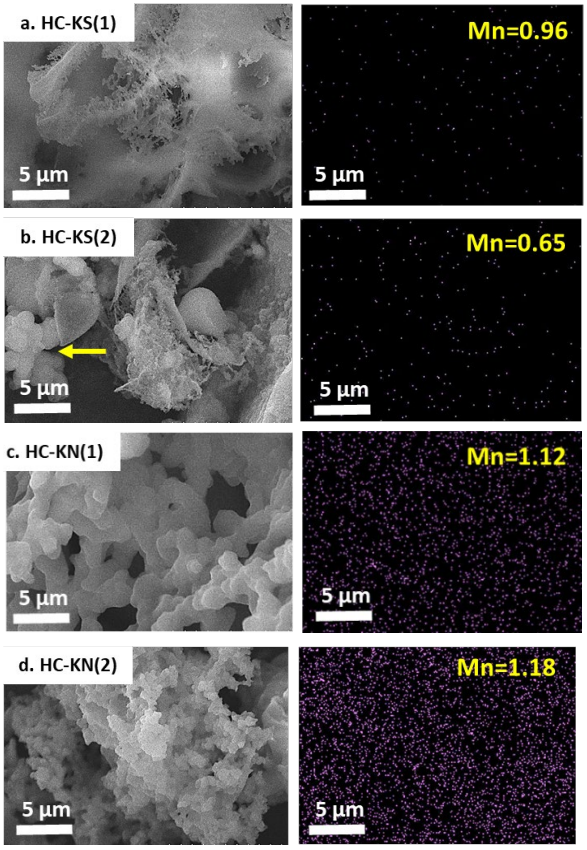

Fig. 2: SEM images of hydrochar samples

Other things seem different in terms of hydrochar morphology when using the $KMnO_4$-NH_4OH catalyst

between one- and two-step heating HTC (Fig. 2 c-d). The samples of HC-KN(1) and HC-KN(2) has a 3D porous networking morphology with uniformly distributed pores. Because of porous particle formation, $KMnO_4$-H_2SO_4 liberates a larger amount of energy to decompose biomass than $KMnO_4$-NH_4OH solution. In an acidic environment, H^+ ions can act as hydrolysis catalysts and create porosity in the solid products. Consequently, the HTC process with acid-assisted conditions will produce hydrochar with a larger pore volume [4,9].

Furthermore, from energy dispersive X-ray analysis (EDX) analysis data, manganese (Mn) is predicted to have a MnO_2 structure in all samples as a result of the reduction of $KMnO_4$ by lignin from the raw material used [21,22]. The higher MnO_2 content of two-step than one-step hydrochar is a crucial aspect that can enhance the electrocapacitance and electrocatalysis of hydrochar [23], as explained in the following section.

3.5 Analysis of Surface ar and Pore Characteristics

To support the pore characteristic discussion above, adsorption-desorption data is provided. As expected, based on the morphology and pores structure in SEM images previously, the two-step hydrochar has a larger specific surface area than the one-step hydrochar in both acidic and alkaline solutions.

There are some points to observe based on the results (Table 3). When the pore size is considered, the one-step hydrochar has a smaller pore size, but the total pore volume formed is also significantly lower than that of the two-step hydrochar. Consequently, the SSA of two-step hydrochar is higher than that of one-step hydrochar. This is due to more intense hydrolysis and chain breaking of soluble components at the prolonged temperature of 100 °C as the first mechanism of HTC [9]. In addition, the presence of material pores leads to enhance the electrochemical performance because the pores of hydrochar are filled with manganese oxide element [24].

Adsorption-desorption isotherm curve in linear plot of the hydrochar (Fig. 3 a-b) shows that the two-step hydrochar revealed an isotherm curve type IV with a narrow hysteresis, represents mesopores structure existences. The data of pores size distribution (Fig. 3 c) of HC-KS(2) and HC-KN(2) were centered at 3.413 and 3.029 nm, respectively.

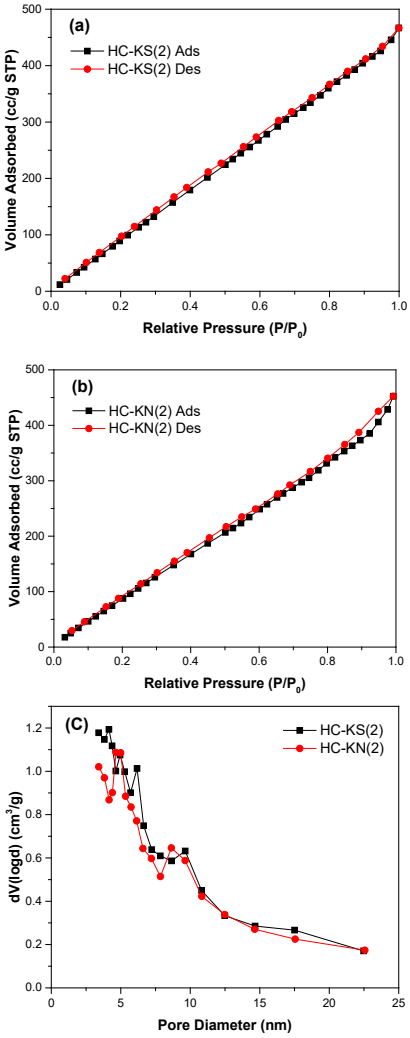

Fig. 3: Aadsorption-desorption isotherm profile (a-b); pore size distribution (c).

Table 3. SSA and Pore Characteristics of Hydrochars

Samples	SSA (m^2/g)	Pore Size (nm)	Pore Volume (cm^3/g)
HC - KS(1)	486.71	3.238	0.394
HC - KS(2)	656.163	3.413	0.618
HC - KN(1)	572.99	2.613	0.247
HC - KN(2)	781.187	3.029	0.678

3.6 Crystallography Patterns of Hydrochar

The XRD patterns of hydrochar in the one- and two-step heating HTC processes are presented in Fig. 4 for HC-KS and HC-KN. The natural structures of carbon can be attributed to the broad C (002) diffraction peak (2θ = 15-30°) [25]. The patterns of both have characteristic peaks that can be carefully observed at 12.9° (110), 18.34 (200), 26.2 (200), 37.6° (211), and 60.26° (521) and are related to the standard of JCPDS 00-044-0141for α-MnO_2. This result shows that α-MnO_2 was successfully synthesized and composited in hydrochar samples. Although these standard characteristic peaks of α-MnO_2 are unclear, they have a broad pattern and an absence of sharp peak suggests that the amorphous structure is dominant [26].

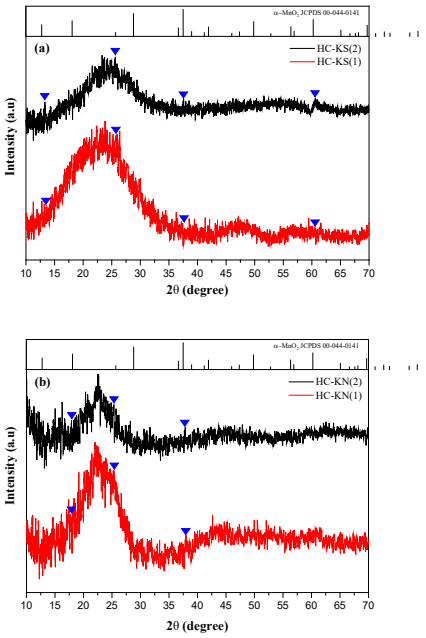

Fig. 4: Crystallography pattern of hydrochar samples

3.7 Chemical Functional Groups Analysis

The FTIR is performed to observe the functional groups of the hydrochar obtained (Fig. 5). The bands found in the spectral region of 900 to 400 cm^{-1} reveal the rich-spectral responses of organic compounds variety, demonstrating the organic substances on the material's surface was complex [27]. Peak intensity decreases at a range of 3000-3700 cm^{-1} in two-step heating of hydrochar, which is related to stretching vibration of the -OH group and hydrophilic content [28,29].

Moreover, the longer retention time of hydrolysis in the two-step heating process leads to the loss of the -OH functional group. The significant decrease in the intensity of -OH bonds also indicates the dehydration phase, which causes the biomass to be entirely dried [30,31]. The signal at 1695 cm^{-1} and 1612 cm^{-1} attributed to the vibration of C=C and C-O aromatic respectively [9,10,27]. The low-intensity bands at approximately 1580 cm^{-1} indicate the overlapping bands of C=C, C=O, and C=N in the HC-KN sample [32]. The region between 1100-1440 cm^{-1} is also assigned as functional Group C-N which significantly increased at high temperatures for a more prolonged reaction [32–34].

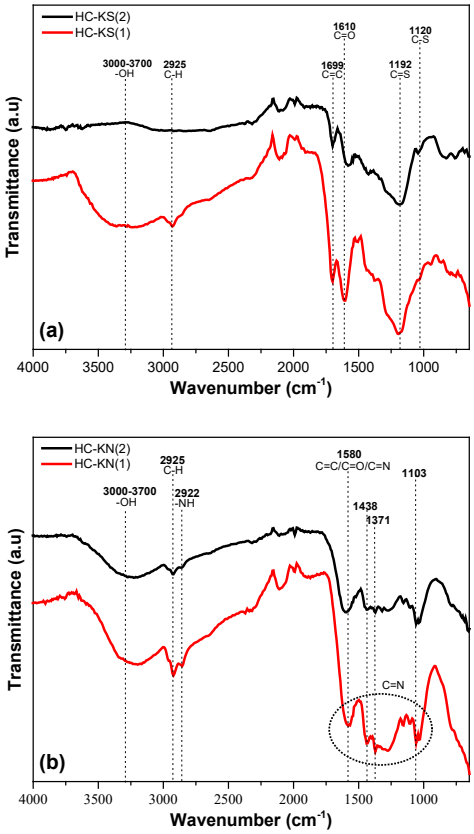

Fig. 5: FTIR spectra of hydrochar in different heating steps of the HTC process.

3.8 Electrocapacitive Activity of Hydrochar

Fig. 6 shows an electrocapacitive test of hydrochar in 0.1 M $Na_2S_2O_3$ at a scan rate of 10 mV/s. The quantitative parameters of the hydrochar's specific capacitance, specific energy, and specific power (Table 4) were calculated using obtained CV data Eq. 1-3 as detailed below:

$$\boldsymbol{Cs} = \frac{\int \boldsymbol{IdV}}{\boldsymbol{2msR}} \quad (1)$$

$$\boldsymbol{E_S^{CV}} = \frac{1}{2}\boldsymbol{C_S}(\Delta \boldsymbol{V})^2 \quad (2)$$

$$\boldsymbol{P_S} = \frac{1}{2}\boldsymbol{C_S}(\Delta \boldsymbol{V})\boldsymbol{r} \quad (3)$$

where $\boldsymbol{C_S}$ is specific capacitance, $\boldsymbol{E_S^{CV}}$ is specific energy, and $\boldsymbol{P_S}$ is specific power. Moreover, $\boldsymbol{I}$ is the current of cathodic (*ampere*), $\boldsymbol{V}$ is potential applied (*volt*), $\boldsymbol{m}$ is samples mass (*gram*), $\boldsymbol{s}$ is rate of scan (*volt/s*), and R is applied potential scan range [35]. Then, $\boldsymbol{\Delta V}$ is difference of voltage and $\boldsymbol{r}$ is potential sweep rate [36].

According to the results, HC-KS(2) has a significantly higher specific capacitance value than HC-KS(1). In contrast, the difference between HC-KN(1) and (HC-KN (2) is not significantly different. The highest specific capacitance value was obtained by HC-KN(2), which was 86.76 F/g. HC-KN(2) also has the highest specific energy

and power value, which both increase proportionately to the specific capacitance value. The highest specific capacitance value of HC-KN(2) is followed by the highest specific surface area referred to in the BET results above. This proves that the surface area of a carbon-based electrode directly influences ion diffusion into its pores, increasing its electrocapacity [37].

Table 4. Calculation data of C_S , E_S^{CV}, P_S of hydrochar from various feedstock solutions and HTC heating-steps.

Sample	Cs (F/g)	E_S^{CV} (10^3).(W/kg)	P_S (10^3) (W·h/kg)
HC – KS(1)	38.06	48.72	0.30
HC - KN(1)	71.22	91.16	0.57
HC - KS(2)	73.54	94.13	0.59
HC - KN(2)	86.76	111.05	0.69

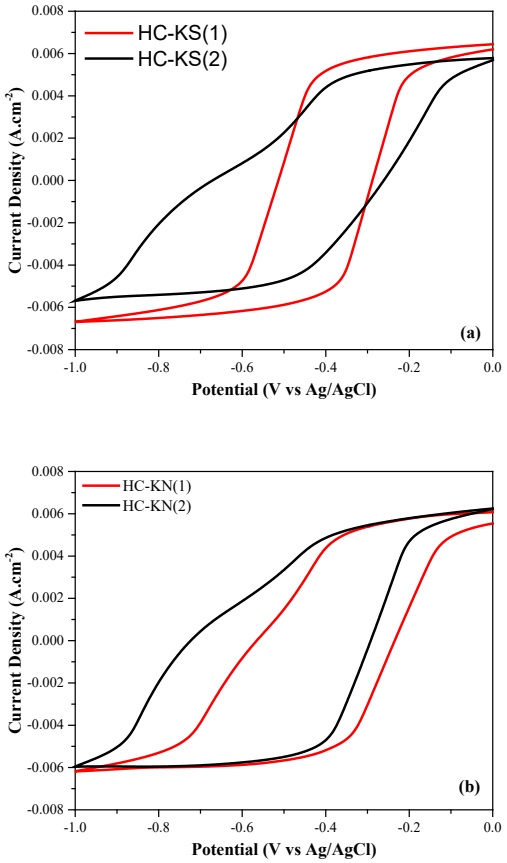

Fig.6: Cyclicvoltammogram of hydrochar in different solution and condition.

3.8 Electrocatalytic Activity of Hydrochar

The electrocatalytic activity potential of hydrochar toward the ORR mechanism is depicted in Fig. 7. The cyclic voltammograms of all hydrochar in N_2-saturated electrolyte (dashed lines) show no reduction peak. In O_2-saturated electrolyte, HC-KS and HC-KN have a reduction peak at -0.365 V (solid lines). These findings unquestionably indicate that the reduction peak was driven by the ORR electrocatalytic activity.

However, the current density of hydrochar produced by a two-step heating process is significantly lower than that of the one-step hydrochar produced. The current density of HC-KS(2) is 0.28 mA/cm^2, which is lower than that of HC-KS(1) with a value of 0.45 mA/cm^2. The HC-KN sample exhibits the same trend, with current densities of 2.15 and 1.49 mA/cm^2 for HC-KN(1) and HC-KN(2), respectively. Using $KMnO_4$-NH_4OH as a feedstock solution in a one- and two-step heating process produces hydrochar with a higher current density than $KMnO_4$-H_2SO_4.

LSV analysis (Fig. 7 c-f) at rotating rates of RDE ranging from 400 - 2800 rpm was used to conduct additional research on ORR kinetics and the electrocatalytic process. The LSV was measured in O_2-saturated electrolyte of 0.1 M KOH with a scan rate of 10 mV/s and applied potential of -0.6-0 V. Because the speed of oxygen flux on the electrode surface increased with rotation speed, the density of diffusion limiting current increased.

The kinetics of ORR mechanism of hydrochar were then investigated using Koutecky-Levich plots. K-L plots (Fig. 8 a-d) has a linear relationship between i^{-1} and $\omega^{-1/2}$. The first-order reaction kinetics are revealed by the linearity of the potential range of -0.4 to -0.5 [38].

In addition, line slope is used for calculating n, using the Koutecky-Levich equation (Eq. 4-6) [12].

$$\frac{1}{i} = \frac{1}{B\omega^{1/2}} + \frac{1}{I_K} \quad (4)$$

$$B = 0.201nFC_{O_2}{D_{O_2}}^{2/3}v^{-1/6} \quad (5)$$

Where i is current density (mA/cm^2), ω is RDE angular velocity (rpm), I_K is kinetic current density (mA/cm^2), n is electrons transferred number per oxygen molecule, F is Faraday constant (96485.33 C.mol^{-1}), D_{O_2} is diffusion coefficient of O_2 molecules in 0.1 M KOH electrolyte (1.9 x 10^{-5} cm^2/s), and v is kinematic viscosity of the electrolyte (1.1 x 10^{-2} cm^2/s). The concentration of O_2, C_{O_2}, was determined as follows Eq. (6) [32]:

$$log\, C_{O_2} = log\, 1.26\, x\, 10^{-3} - 0.1746C_{KOH} \quad (6)$$

Table 5. Calculation data of (I_K) and (n)

Samples	I_k (mA/cm^2)	n
HC - KS(1)	0.07	1.83
HC - KS(2)	0.36	1.82
HC - KN(1)	0.96	2.21
HC - KN(2)	0.32	3.88

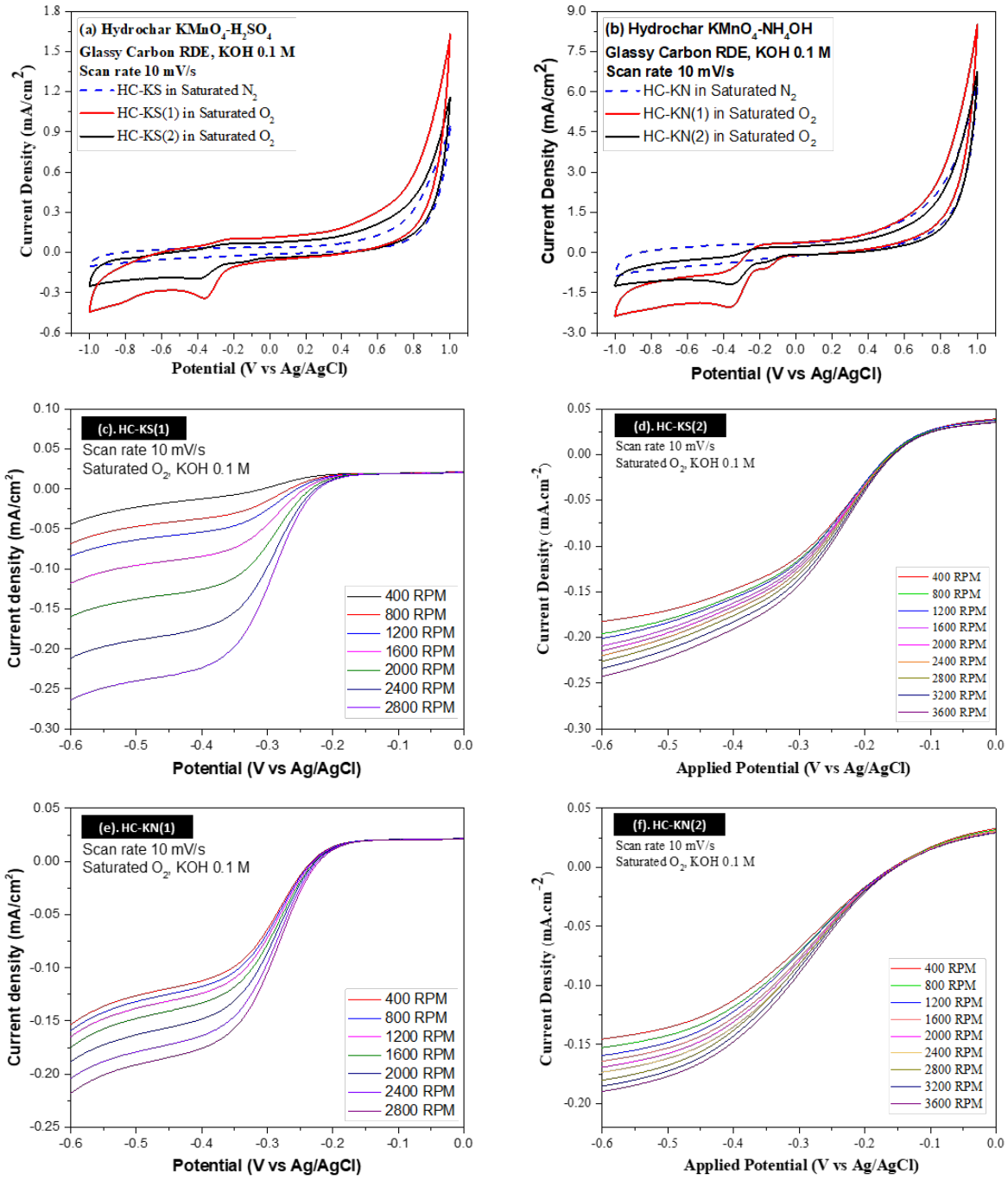

Fig. 7: Cyclic voltammogram in O_2- and N_2- saturated electrolyte (a-b); Linear sweep voltammetry (c-f)

Table 5 display the data of the (I_K) and (n) for the hydrochar. Hydrochar produced from one and two steps generates different electrocatalytic activities. Evaluated from the I_K and n results, the use of $KMnO_4$-NH_4OH as a feedstock solution successfully produces hydrochar with a better ORR electrocatalytic capability during one- and two-step heating of the HTC process. These results follow the same pattern as the electrocapacitive value, in which using two-step heating can enhance the electrocatalytic activity of the obtained hydrochar.

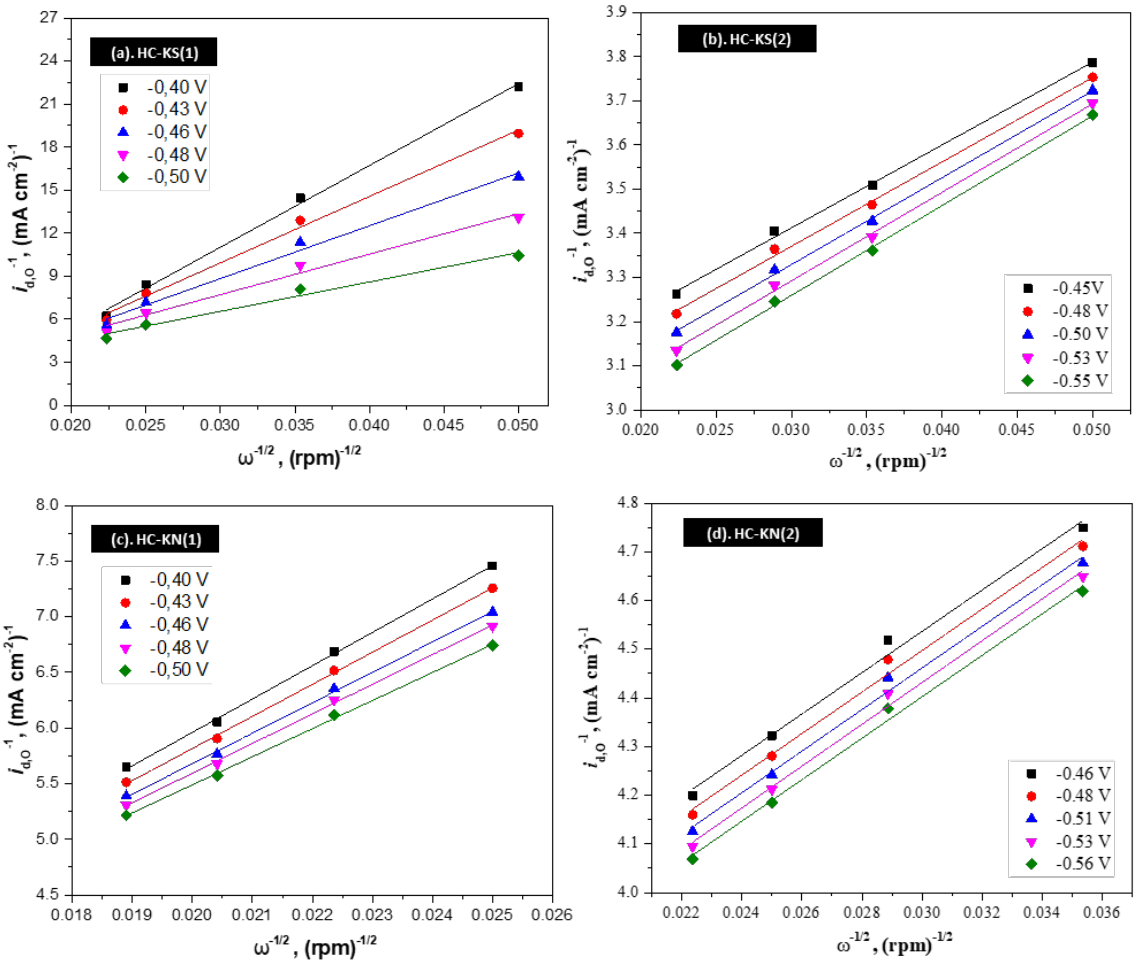

Fig. 8: K-L plots of HC-KS(1) (a); HC-KS(2) (b); HC-KN(1) (c); and HC-KN(2) (d)

The electrons transferred number of HC-KN(1) was 2.21 (n ≈ 2) in ORR test, represent that ORR occurs via a two-electron pathway, as given in Eqs. Eq. 7-8 below: [39]:

$$O_2 + H_2O + 2e^- \rightarrow HO_2^- + OH^- \quad (7)$$

$$HO_2^- + H_2O + 2e^- \rightarrow 3OH^- \quad (8)$$

On the other hand, the electrons transferred number for HC-KN(2) was 3.88 (n ≈ 4), so the ORR mechanism follows a four-electron pathway (Eq. 9):

$$O_2 + 2H_2O + 4e^- \leftrightarrow 4OH^- \quad (9)$$

Even though the electrons transferred number is higher for HC-KN(2) than for HC-KN(1), the kinetic current density produced by HC-KN(2) is less than that of HC-KN(1), as shown in Table 5.

3.9 HTC Process Mechanism of One- and Two-step Heating and its Influence on Hydrochar Characteristics

The following paragraph will discuss the difference in the hydrochar formation mechanism from lignocellulosic biomass through one- and two-step processes. It will also explain and answer why the two-step HTC process more efficiently produces hydrochar with better characteristics and electrochemical performance in both acidic and alkaline solutions, as reported before. HTC is linked to consecutive processes involving biomass components as well as hydrolysis, condensation, dehydration, decarboxylation, polymerization, and aromatization stage [40]. It is worthy to note that a complex series of reactions occurred and were influenced by various factors. In addition to the operating conditions of HTC, biomass components as raw materials also affect hydrochar characteristics [41]. Since different biomasses contain varying components insides, the reactions that occur during the formation of hydrochar are also different for each of the raw materials used. Fig. 9 illustrates the scheme of hydrochar formation from lignocellulosic components through the HTC process.

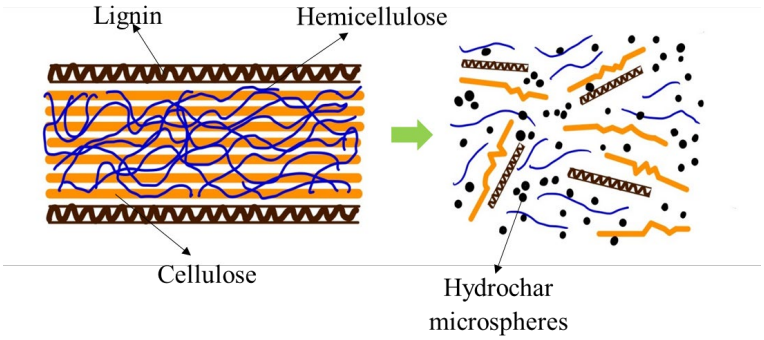

Fig. 9: Schematic illustration of the formation of hydrochar from lignocellulosic biomass

In the HTC process, liquid and volatile byproducts are formed by hydrolysis and/or dehydration of lignocellulosic biomass as the first stage. This is the key reason why one- and two-step heating resulted in hydrochar with significantly different characteristics and performances. At this stage, the mass drops rapidly in a short time. The liquid product was polymerized and condensed during the HTC process. For this reason, several studies have found that a longer HTC reaction time is preferable for producing solid hydrochar [9,42].

Furthermore, natural cellulose and lignin structures are destroyed. During this step, a heterogeneous pyrolysis-like process occurred, resulting in polyaromatic char formation with a connecting-porous structure. In other words, hydrochar is formed not only through a series of processes but also through solid-to-solid conversion of insoluble lignocellulosic components at a specific temperature. More details of the hydrochar formation mechanism and its reaction pathway from lignin, cellulose, and hemicellulose are presented in Fig. 10.

Lignin, cellulose, and hemicellulose decomposition temperatures differ for hydrochar formation. During the HTC process, hemicellulose and cellulose dissolve and hydrolyze at temperatures ranging from 170-180 °C. Meanwhile, lignin is the most challenging component to dissolve and convert to hydrochar. The hydrolysis of lignin in the HTC process begins at 200 °C, and only a tiny portion of the lignin can be hydrolyzed using water. The entire reaction stage continues as the reaction time during the HTC process [40].

In this study, $KMnO_4$ is primarily used as a source of a nonnoble metal oxide, MnO_2, which can improve the electrochemical performance of hydrochar. As previously discussed, $KMnO_4$ can also function as an oxidizing agent, opening the aromatic ring of lignin, which is crucial in the decomposition of biomass components.

On the other hand, solid-to-solid conversion of lignocellulosic components into solid hydrochar spontaneously occurred at temperatures from 170 °C through the pyrolysis-like stage during the HTC process.

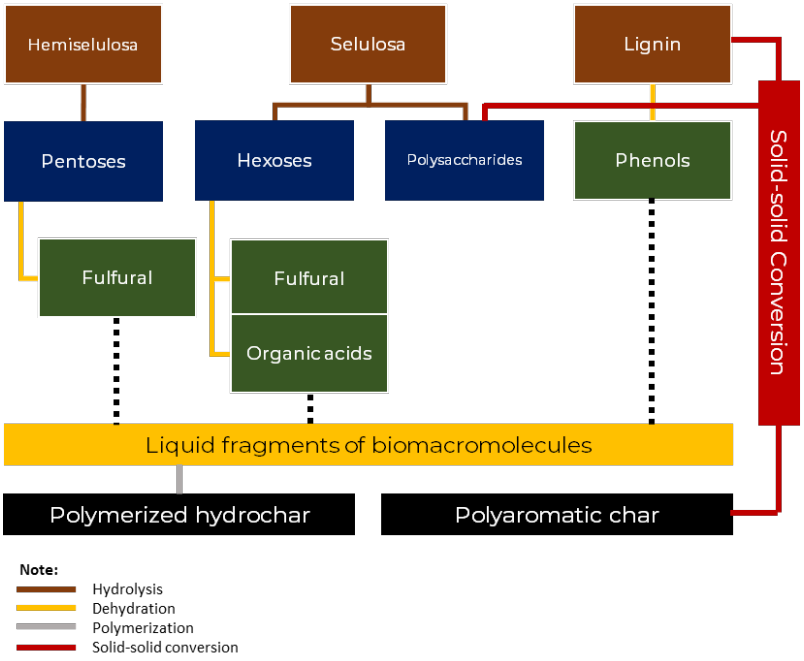

Fig. 10: Mechanism and reaction pathway of hydrochar formation from lignocellulosic biomass

Therefore, it can be a disadvantage in one-step heating HTC to produce materials with good electrochemical performance. Once the target temperature of 200 °C is reached, solid-to-solid lignin conversion can occur spontaneously and form hydrochar spheres. The conversion of lignin to hydrochar will disrupt the lignin function in reducing $KMnO_4$ to MnO_2. As a result, dividing the HTC process into two heating processes may be a promises strategy to increase the electrochemical performance of the resulting hydrochar.

In the HTC process with two-step heating, the temperature was set at 100 °C for 4 h and then continued at 200 °C for 8 h. When the initial set point temperature of 100 °C is reached, the thermochemical conversion process of the biomass component is confirmed to not achieve hydrochar formation, either through solid–liquid or solid–solid conversion. However, at 100 °C, the lignin dissolving process in acid or alkaline conditions occurs, known as delignification. The presence of unconverted lignin can contribute to reducing $KMnO_4$ to MnO_2. The process continues until the temperature reaches 200 °C, where the lignocellulosic components can be converted into hydrochar with hydrochar- MnO_2 composite formation simultaneously.

4. Conclusion

Using a one- and two-step HTC procedure, a hydrochar-MnO2 composite was successfully synthesized from extracted avocado seed. in acidic and basic catalyst medium. Hydrochar obtained from two-step heating HTC with NH_4OH catalyst has the highest value of specific capacitance of 86.76 F/g. Furthermore, the ORR study showed the transferred-electron number and kinetic current density values of 3.88 and 0.32 mA/cm^2, respectively. These results imply that different catalysts and heating steps of HTC can modify the reaction mechanism of the simultaneous hydrochar and MnO_2 formation.

Acknowledgments

This present study was supported by the Ministry of Education, Culture, Research, and Technology, Indonesia, through the research grant (Main Contract No. 009/E5/PG.02.00.PL/2023 12 April 2023 and Derivative Contract No. 1257/PKS/ITS/2023 13 April 2023). Furthermore, we thank the PMDSU program for providing a doctoral scholarship to one of the authors (S.T.). In addition, we thank Ms. Zahrinne Aliefia Firdaus and Mr. Pungky Triwiya Nugraha for their assistance during the experiments.

Nomenclature

EASP	Extracted Avocado Seed Powder
CV	Cyclic Voltammetry
HC-KN	Hydrochar with $KMnO_4$-NH_4OH feedstock solution
HC-KS	Hydrochar with $KMnO_4$-H_2SO_4 feedstock solution
ORR	Oxygen Reduction Reaction

References

1) T.B. Bahru, Z.H. Tadele, and E.G. Ajebe, "A review on avocado seed: functionality, composition, antioxidant and antimicrobial properties," *Chem. Sci. Int. J.*, 1–10 (2019). doi:10.9734/csji/2019/v27i230112.

2) R.K. Ahmad, S.A. Sulaiman, A.M.B.A. Majid, S. Yusuf, S.S. Dol, M. Inayat, and H.A. Umar, "Assessing the technical and environmental potential of coconut shell biomass: experimental study through pyrolysis and gasification," *Evergreen*, 10 (*1*) 585–593 (2023). doi:10.5109/6782165.

3) J. Waluyo, M.M. Setianto, N.R. Safitri, S.H. Pranolo, A.D. Susanti, Margono, and Paryanto, "Characterization of biochar briquettes from coconut shell with the effect of binder: molasses, cow manure and horse manure," *Evergreen*, 10 (*1*) 539–545 (2023). doi:10.5109/6782158.

4) Y. Li, A. Meas, S. Shan, R. Yang, X. Gai, H. Wang, and N. Tsend, "Hydrochars from bamboo sawdust through acid assisted and two-stage hydrothermal carbonization for removal of two organics from aqueous solution," *Bioresour. Technol.*, 261 257–264 (2018). doi:10.1016/j.biortech.2018.03.108.

5) R.H. Fitri Faradilla, L. Lucia, and M. Hakovirta, "Hydrothermal carbonization of soybean hulls for the generation of hydrochar: a promising valorization pathway for low value biomass," *Environ. Nanotechnology, Monit. Manag.*, 16 (*March*) 100571 (2021). doi:10.1016/j.enmm.2021.100571.

6) M.T. Reza, E. Rottler, L. Herklotz, and B. Wirth, "Hydrothermal carbonization (htc) of wheat straw: influence of feedwater ph prepared by acetic acid and potassium hydroxide," *Bioresour. Technol.*, 182 336–344 (2015). doi:10.1016/j.biortech.2015.02.024.

7) G.A.G. Kavindi, Z. Lei, T. Yuan, K. Shimizu, and Z. Zhang, "Use of hydrochar from hydrothermal co-carbonization of rice straw and sewage sludge for cr(vi) bioremediation in soil," *Bioresour. Technol. Reports*, 18 101052 (2022). doi:10.1016/j.biteb.2022.101052.

8) S.T.W. Amelia, T. Nurtono, H. Setyawan, and W. Widiyastuti, "Electrocapacitive and electrocatalytic performances of hydrochar prepared by one-step hydrothermal carbonization without further activation," *Mater. Res. Express*, 10 (*7*) 075602 (2023). doi:10.1088/2053-

1591/ace75f.

9) Y. Lei, H. Su, and R. Tian, "Morphology evolution, formation mechanism and adsorption properties of hydrochars prepared by hydrothermal carbonization of corn stalk," *RSC Adv.*, 6 (*109*) 107829–107835 (2016). doi:10.1039/c6ra21607b.

10) A. Jain, R. Balasubramanian, and M.P. Srinivasan, "Hydrothermal conversion of biomass waste to activated carbon with high porosity: a review," *Chem. Eng. J.*, 283 789–805 (2016). doi:10.1016/j.cej.2015.08.014.

11) M.F. Rois, S. Ramadhani Alya Sasono, W. Widiyastuti, T. Nurtono, and H. Setyawan, "High-performance electrocatalyst made from lignosulfonate nanofiber composited with manganese dioxide without carbonation process," *Adv. Powder Technol.*, 33 (*5*) 103572 (2022). doi:10.1016/j.apt.2022.103572.

12) M. Mahmudi, W. Widiyastuti, P. Nurlilasari, S. Affandi, and H. Setyawan, "Manganese dioxide nanoparticles synthesized by electrochemical method and its catalytic activity towards oxygen reduction reaction," *J. Ceram. Soc. Japan*, 126 (*11*) 906–913 (2018). doi:10.2109/jcersj2.18091.

13) H. Purwaningsih, N.M.I.P. Suari, W. Widiyastuti, and H. Setyawan, "Preparation of rgo/mno 2 composites through simultaneous graphene oxide reduction by electrophoretic deposition," *ACS Omega*, 7 (*8*) 6760–6767 (2022). doi:10.1021/acsomega.1c06297.

14) A.H. Wibowo, H. Al Arraf, A. Masykur, F. Rahmawati, M. Firdaus, F. Pasila, U. Farahdina, and N. Nasori, "Composite of polyaniline/reduced graphene oxide with the single-, bi- and tri- metal oxides modification and the effect on the capacitance properties," *Evergreen*, 10 (*1*) 85–93 (2023). doi:10.5109/6781053.

15) D.B. Kautsar, M.F. Rois, N. Faizah, W. Widiyastuti, T. Nurtono, and H. Setyawan, "Antioxidant and antimicrobial agents from avocado (persea americana) seed extract encapsulated in gum arabic through spray drying method," *Period. Polytech. Chem. Eng.*, (2023). doi:10.3311/PPch.20698.

16) R. Datta, "Acidogenic fermentation of lignocellulose–acid yield and conversion of components," *Biotechnol. Bioeng.*, 23 (*9*) 2167–2170 (1981). doi:10.1002/bit.260230921.

17) J.A. Dávila, M. Rosenberg, E. Castro, and C.A. Cardona, "A model biorefinery for avocado (persea americana mill.) processing," *Bioresour. Technol.*, 243 17–29 (2017). doi:10.1016/j.biortech.2017.06.063.

18) D. Merino, L. Bertolacci, U.C. Paul, R. Simonutti, and A. Athanassiou, "Avocado peels and seeds: processing strategies for the development of highly antioxidant bioplastic films," *ACS Appl. Mater. Interfaces*, 13 (*32*) 38688–38699 (2021). doi:10.1021/acsami.1c09433.

19) S.P. Bangar, K. Dunno, S.B. Dhull, A. Kumar Siroha, S. Changan, S. Maqsood, and A.V. Rusu, "Avocado seed discoveries: chemical composition, biological properties, and industrial food applications," *Food Chem. X*, 16 100507 (2022). doi:10.1016/j.fochx.2022.100507.

20) S. Puncha-arnon, Y. Wandee, D. Uttapap, C. Puttanlek, and V. Rungsardthong, "The effect of hydrolysis of cassava starch on the characteristics of microspheres prepared by an emulsification-crosslinking method," *Int. J. Biol. Macromol.*, 161 939–946 (2020). doi:10.1016/j.ijbiomac.2020.06.122.

21) M. Fauziyah, W. Widiyastuti, R. Balgis, and H. Setyawan, "Production of cellulose aerogels from coir fibers via an alkali–urea method for sorption applications," *Cellulose*, 26 (*18*) 9583–9598 (2019). doi:10.1007/s10570-019-02753-x.

22) M.F. Rois, S. Ramadhani Alya Sasono, W. Widiyastuti, T. Nurtono, and H. Setyawan, "High-performance electrocatalyst made from lignosulfonate nanofiber composited with manganese dioxide without carbonation process," *Adv. Powder Technol.*, 33 (*5*) 103572 (2022). doi:10.1016/j.apt.2022.103572.

23) Y. Iriani, R. Afriani, D.K. Sandi, and F. Nurosyid, "Co-precipitation synthesis and photocatalytic activity of mn-doped srtio3for the degradation of methylene blue wastewater," *Evergreen*, 9 (*4*) 1039–1045 (2022). doi:10.5109/6625717.

24) F. Taufany, M.J. Pasaribu, B.Y.S. Romaji, Y. Rahmawati, A. Altway, Susianto, S. Nurkhamidah, J.G. Anfias, Y. Mursidah, D. Fujanita, S. Yulianti, D. Rahmawati, and G. Stellarosari, "The synthesis of activated carbon from waste tyre as fuel cell catalyst support," *Evergreen*, 9 (*2*) 412–420 (2022). doi:10.5109/4794166.

25) M. Kaur, N. Mittal, A. Charak, A.P. Toor, and V. Singh, "Rice husk derived activated carbon for the adsorption of scarlet rr an anionic disperse dye," *Evergreen*, 10 (*1*) 438–443 (2023). doi:10.5109/6782146.

26) H.-M. Lee, H.-R. Kang, K.-H. An, H.-G. Kim, and B.-J. Kim, "Comparative studies of porous carbon nanofibers by various activation methods," *Carbon Lett.*, 14 (*3*) 180–185 (2013). doi:10.5714/cl.2013.14.3.180.

27) M.S. Santana, R.P. Alves, L.S. Santana, M.A. Gonçalves, and M.C. Guerreiro, "Structural, inorganic, and adsorptive properties of hydrochars obtained by hydrothermal carbonization of coffee waste," *J. Environ. Manage.*, 302 (*October 2021*) (2022). doi:10.1016/j.jenvman.2021.114021.

28) S. Singh, L. Nagdeve, H. Kumar, and K. Dhakar,

"Rice straw based natural fiber reinforced polymer for sustainable bio- composites: a systematic review," *Evergreen*, 10 (*2*) 1041–1052 (2023). doi:10.5109/6793661.

29) V. Ordonez, H. Baykara, A. Riofrio, M. Cornejo, and R. Rodríguez, "Preparation and characterization of ecuadorian bamboo fiber-low-density polyethylene (ldpe) biocomposites," *Evergreen*, 10 (*1*) 43–54 (2023). doi:10.5109/6781037.

30) M. Sevilla, and A.B. Fuertes, "The production of carbon materials by hydrothermal carbonization of cellulose," *Carbon N. Y.*, 47 (*9*) 2281–2289 (2009). doi:10.1016/j.carbon.2009.04.026.

31) M. Wortmann, W. Keil, B. Brockhagen, J. Biedinger, M. Westphal, C. Weinberger, E. Diestelhorst, W. Hachmann, Y. Zhao, M. Tiemann, G. Reiss, B. Hüsgen, C. Schmidt, K. Sattler, and N. Frese, "Pyrolysis of sucrose-derived hydrochar," *J. Anal. Appl. Pyrolysis*, 161 (*November 2021*) 105404 (2022). doi:10.1016/j.jaap.2021.105404.

32) M. Fauziyah, W. Widiyastuti, and H. Setyawan, "Nitrogen-doped carbon aerogels prepared by direct pyrolysis of cellulose aerogels derived from coir fibers using an ammonia–urea system and their electrocatalytic performance toward the oxygen reduction reaction," *Ind. Eng. Chem. Res.*, 59 (*49*) 21371–21382 (2020). doi:10.1021/acs.iecr.0c03771.

33) S. Nayak, L. Mohapatra, and K. Parida, "Visible light-driven novel g-c3n4/nife-ldh composite photocatalyst with enhanced photocatalytic activity towards water oxidation and reduction reaction," *J. Mater. Chem. A*, 3 (*36*) 18622–18635 (2015). doi:10.1039/c5ta05002b.

34) A. Alowasheeir, S. Tominaka, Y. Ide, Y. Yamauchi, and Y. Matsushita, "Two-dimensional cyano-bridged coordination polymer of mn(h2o)2[ni(cn)4]: structural analysis and proton conductivity measurements upon dehydration and rehydration," *CrystEngComm*, 20 (*42*) 6713–6720 (2018). doi:10.1039/c8ce01400k.

35) F. Fahmi, N.A.A. Dewayanti, W. Widiyastuti, and H. Setyawan, "Preparation of porous graphene-like material from coconut shell charcoals for supercapacitors," *Cogent Eng.*, 7 (*1*) 1748962 (2020). doi:10.1080/23311916.2020.1748962.

36) R. Holze, "S. ratha, a.k. samantara: supercapacitor: instrumentation, measurement and performance evaluation techniques, xvii + 52 p. springer, singapore 2018, 58.84 €; isbn: 978-981-13-3085-8," *J. Solid State Electrochem.*, 25 (*7*) 2143–2143 (2021). doi:10.1007/s10008-021-04970-6.

37) S. Ghosh, R. Santhosh, S. Jeniffer, V. Raghavan, G. Jacob, K. Nanaji, P. Kollu, S.K. Jeong, and A.N. Grace, "Natural biomass derived hard carbon and activated carbons as electrochemical supercapacitor electrodes," *Sci. Rep.*, 9 (*1*) (2019). doi:10.1038/s41598-019-52006-x.

38) Q. Shao, J. Liu, Q. Wu, Q. Li, H. guo Wang, Y. Li, and Q. Duan, "In situ coupling strategy for anchoring monodisperse co 9 s 8 nanoparticles on s and n dual-doped graphene as a bifunctional electrocatalyst for rechargeable zn–air battery," *Nano-Micro Lett.*, 11 (*1*) 1–14 (2019). doi:10.1007/s40820-018-0231-3.

39) R. Ma, G. Lin, Y. Zhou, Q. Liu, T. Zhang, G. Shan, M. Yang, and J. Wang, "A review of oxygen reduction mechanisms for metal-free carbon-based electrocatalysts," *Npj Comput. Mater.*, 5 (*1*) (2019). doi:10.1038/s41524-019-0210-3.

40) T. Wang, Y. Zhai, Y. Zhu, C. Li, and G. Zeng, "A review of the hydrothermal carbonization of biomass waste for hydrochar formation: process conditions, fundamentals, and physicochemical properties," *Renew. Sustain. Energy Rev.*, 90 (*December 2016*) 223–247 (2018). doi:10.1016/j.rser.2018.03.071.

41) M. Heidari, S. Salaudeen, P. Arku, B. Acharya, S. Tasnim, and A. Dutta, "Development of a mathematical model for hydrothermal carbonization of biomass: comparison of experimental measurements with model predictions," *Energy*, 214 119020 (2021). doi:10.1016/j.energy.2020.119020.

42) H.B. Sharma, S. Panigrahi, and B.K. Dubey, "Hydrothermal carbonization of yard waste for solid bio-fuel production: study on combustion kinetic, energy properties, grindability and flowability of hydrochar," *Waste Manag.*, 91 108–119 (2019). doi:10.1016/j.wasman.2019.04.056.